Applied Catalysis B: Environmental 256 (2019) 117780

Contents lists available at ScienceDirect

Applied Catalysis B: Environmental

journal homepage: www.elsevier.com/locate/apcatb

# Modeling the effect of Cu doped $TiO_2$ with carbon dots on $CO_2$ methanation by $H_2O$ in a photo-thermal system

Ke Wang[a], Ruimin Jiang[a,b], Ting Peng[a,b], Xu Chen[a], Wenxin Dai[a,b,*], Xianzhi Fu[a,*]

[a] Research Institute of Photocatalysis, State Key Laboratory of Photocatalysis on Energy and Environment, Fuzhou University, Fuzhou, 350002, China
[b] Key Laboratory of Eco-Materials Advanced Technology, Fuzhou University, Fujian, Fuzhou, 350002, China

ARTICLE INFO

*Keywords:*
$CO_2$ reduction
Photo-thermal catalysis
Carbon dots
Cu(I)/Cu(II)

ABSTRACT

The process of $CO_2$ reduction by $H_2O$ is always restricted due to its non-spontaneous in thermodynamic. In this work, a photo-thermal coupled device is designed to obtain a high-achievement $CO_2$ methanation by $H_2O$ over carbon dots (CDs) drafted Cu/$TiO_2$ (Cu/$TiO_2$-C). Dramatic promotion of $CH_4$ production exhibits under UV irradiation at a higher temperature (> 150 °C), but a poor photo-promotion at room temperature. In-situ diffuse reflectance infrared Fourier transform spectroscopy (DRIFTS) and isotopic-label temperature programmed surface reaction (TPSR) suggest that $CO_2$ methanation process over Cu/$TiO_2$-C can be regarded as two main spontaneous process: $CO_2$ is firstly reduced by Cu(I) ($Cu_2O$) to CO ($CO_2 + Cu_2O \rightarrow CO + CuO$), then CO is reduced by $H_2O$ to $CH_4$ via water-gas shift (WGS) process. Here, CDs not only act as electron storage to keep the presence of Cu(I) (from Cu(II) to Cu(I) not to Cu (0)) at a high temperature, but also capture the photo-generated holes from $TiO_2$ induced by UV light, resulting in the cycle of Cu (I)/ Cu(II) with concomitant of electron storage and release. The synergy effect of UV light and temperature do not occur on the Cu/$TiO_2$ sample without CDs. Here, Cu (II) is mainly reduced by $H_2$ pretreatment to Cu (0), while the poor cycle of Cu(I)/Cu(II) was exhibited under UV irradiation. This study shows that this non-spontaneous reaction could be designed as two ongoing spontaneous processes by adding UV light, this approach may apply to other photo-thermal reactions.

## 1. Introduction

The levels of $CO_2$ in the atmosphere have been changing over time due to social development [1]. One crucial constraint on solving the problem of $CO_2$ is that any energy source used should not produce more $CO_2$ [2]. Reduction of $CO_2$ to chemicals using solar energy is considered as a sustainable method. Many reactions, *e.g.* the reduction of $CO_2$ by $H_2$ into chemicals, is applied into the conversion of $CO_2$. These reactions usually occur at a high temperature, owing to fast the $CO_2$ transformation of intermediates, however, these methods would require extra energy input [3–5]. Thus, the reduction of $CO_2$ directly using solar energy is an attractive research. Many works have focused on the reduction of $CO_2$ by water using solar energy, because the regents (water and $CO_2$) are rich in nature [6,7]. For this reaction, many $CO_2$ intermediates transformation have been reported, *e.g.* *C, *COOH species et al [8,9]. Simultaneously, these intermediates transformation require protons participation, and then convert $CO_2$ and water into hydrocarbons and $O_2$ [10,11]. Thus, the reduction of $CO_2$ involves redox reaction including water oxidization to $O_2$ and reduction of $CO_2$ to chemicals. Interestingly, a few narrow-bandgap semiconductors allow simultaneous conversion of $CO_2$ and water into hydrocarbons and $O_2$ efficiently [12–14] because these semiconductors need to own both a suitable VB position (respecting to $H_2O$ oxidation potential) and a wide bandgap larger than 1.35 eV [13]. $TiO_2$ is an alternatively candidate for $CO_2$ reduction, due to its suitable VB and CB position for water oxidizing and $CO_2$ reducing [15]. However, the lower efficient of $CO_2$ reduction exhibits in $TiO_2$-materials [2,16]. Many strategies have been applied to enhance $CO_2$ reduction over $TiO_2$ by doping noble or non-noble metal elements [15,17,18]. Among these metal elements, Cu modified $TiO_2$ materials have been greatly attracted to the conversion of $CO_2$ in various systems [19,20]. Moreover, Cu species in different oxidation states is supposed to act as both sensitizer and a co-catalyst for $TiO_2$ [21]. But, it is still confused which one of Cu(I), Cu(II) or Cu (I)/Cu(II) species would be responsible for excellent activity performance [22]. *e.g.*, some works have been proposed that Cu(I) showed an excellent performance due to the excellent $CO_2$ adsorption and separation charges as hole scavenger [23,24]. Other reports have putted that Cu(II) could promote $CO_2$ conversion into chemicals due to

* Corresponding authors at: Research Institute of Photocatalysis, State Key Laboratory of Photocatalysis on Energy and Environment, Fuzhou University, Fuzhou, 350002, China.
*E-mail addresses:* daiwenxin@fzu.edu.cn (W. Dai), xzfu@fzu.edu.cn (X. Fu).

https://doi.org/10.1016/j.apcatb.2019.117780
Received 21 January 2019; Received in revised form 29 April 2019; Accepted 25 May 2019
Available online 27 May 2019
0926-3373/ 

excellent adsorption of $CO_2$ and other intrinsic properties [25]. In our knowledge, carbon dots (CDs) have been applied into many fields as a novel material [26,27]. Expect for up-conversion photoluminescence, CDs can act electron transporters and acceptors during the reactions [28–30].

Furthermore, photocatalytic efficiency for $CO_2$ reduction by $H_2O$ is still very low [31–34]. Considering that a high temperature is favorable to the activation of reactant molecules, thus an extra heat configuration is introduced into the photocatalytic reaction system of $CO_2$ reduced by $H_2O$ in this work. Here, a CDs drafted $Cu/TiO_2$ catalyst ($Cu/TiO_2$-C) was prepared by a facile method, and reaction system was designed to investigate $CO_2$ reduction by water under the photo-thermal condition. As our expected, this as-prepared sample exhibited an excellent methanation activity under UV irradiation at high temperature. However, to be our unexpected, after a series of characteristics for the sample, it was found that the $CO_2$ reduction over $Cu/TiO_2$-C under UV irradiation seemed not to proceed as a main photocatalytic process, and this non-spontaneous thermodynamic reaction could be regarded as two main spontaneous processes: $CO_2$ was firstly reduced by Cu(I) ($Cu_2O$) to CO and then CO was reduced by $H_2O$ to $CH_4$ via a water-gas shift (WGS) process. The existence of CDs and UV light was mainly favorable for the proceeding of two thermo-catalytic processes by realizing the cycle of Cu(I)/Cu(II) sites. Finally, a possible mechanism was proposed to elucidate the above $CO_2$ reduction by $H_2O$.

## 2. Experimental

### 2.1. Preparation of catalysts

#### 2.1.1. Preparation of CDs

The CDs were prepared as literature. [35] In briefly citric acid (1.05 g) and ethylenediamine (335 μL) was dissolved in DI-water (10 mL). Then the solution was transferred to a poly (tetrafluoroethylene) (Teflon)-lined autoclave (30 mL) and heated at 200 °C for 5 h. After the reaction, the reactors were cooled to room temperature by water or naturally. The product, which was brown-black and transparent, was subjected to dialysis to obtained CDs solution.

#### 2.1.2. Preparation of $Cu/TiO_2$-C, $Cu/TiO_2$-C & $Cu/SiO_2$ samples

The titanium dioxide ($TiO_2$) support was made by hydrothermal method. 10 mL tetra-*n*-butyl titanate was dissolved ethanol into 20 mL ethanol, the light yellow solution was obtained and denoted solution A. Solution B was included 200 mL alcohol and 5 mL deionized water and 5 ml CDs solution, pH value was adjusted to 9.0 using ammonia. Then, the solution A was dropwisely added into the solution B with vigorous stirring. After stirring for 1 h, the solution was transported into 100 ml Teflon-line with stainless autoclave, and heated at 150 °C for 8 h. The precipitant was washed and centrifuged by alcohol and water until pH = 7. The sample was transported into an oven, dried at 80 °C for whole night. The obtained sample (denoted as $TiO_2$-C) contained CDs c.a. 0.3 wt% and Cu c.a. 0.90 wt%, the corresponding detail could be seen in information (seeing Table S1 in supporting information (SI)). The copper was loaded onto the $TiO_2$-C support by using the photo-reduction method, a desired copper nitric solution by calculation (1.0 wt%) was added into a quartz reactor which immerse into $TiO_2$-C powder. 5 ml methanol was added into the reactor, the residual of oxygen was exhausted by pure nitrogen. Xe lamp illumination was induced to the system for 30 min, condensate water was used to cooled the system temperature at 10 °C. After illumination, the sample was obtained by centrifugation and dried at 80 °C. Finally, the sample was grinded and sieved 80~120 meshes. The obtained sample was denoted as ($Cu/TiO_2$-C). In addition, $Cu/TiO_2$ sample was prepared by aforementioned method. The different was that it was free of CDs adding during $TiO_2$ preparation.

$Cu/SiO_2$ sample was prepared with impregnation method. Firstly, $SiO_2$ was obtained from ethyl silicate drying. Then, Cu species were deposited onto the $SiO_2$ with impregnation. Finally, the sample was reduction using $NaBH_4$.

### 2.2. Characterizations of catalysts

X-ray diffractions (XRD) of samples were recorded on Bruke D8 Advance powder X-ray diffractometer operated at 40 mA and 40 KV using Cu Ka radiation. Moreover, the crystalline sized could be obtained by Scherrer equation: $D = (k\lambda/\beta_D\cos\theta)$. Where D was the crystalline size, λ was the wavelength of radiation, k was a constant equal to 0.94, $\beta_D$ was the peak width at half-maximum intensity, and θ was the peak position. UV–vis diffuse reflect spectra (UV–vis DRS) of samples were characterized on Varian Cary500 with $BaSO_4$ as internal reflectance standard. Raman (Invia Reflex 1900099S, excitation at 325 nm) was conducted to further investigate the phase structure of samples. Transmission electron microscopy (TEM) investigations of samples were carried out on a JEOL JEM –2010 EX with 200kv field emission gun. Nitrogen isothermal stripping absorption curves of samples were measured at liquid $N_2$ temperature with a Micromeritics ASAP 2020 BET analyzer after the sample was outgassed at vacuum and 150 °C for 4 h. Elemental Analyses (EA) of samples were tested on Vario EL cube of the Elementar Analysensysteme GmbH. The real amount of copper was conducted by ICP-OES (Aglient, ICP-OES 720) assistant with Deyo Bot Advanced Materials Co., Ltd. X-ray Photoelectron spectroscopy (XPS) of samples was measured on Thermo Scientific ESCALab250 spectrometer with monochromatic Al Ka as X-ray source (1486.60 eV).and with a hemispherical analyzer. The C1 s signal of 284.60 eV was used to calibrate the XPS data.

The electrochemical properties of the samples were performed with an electrochemical analyzer having a three-electrode configuration. A fluorine-doped tin oxide (FTO) conductive glass coated with the material film was used as a working electrode, Pt wire as a counter-electrode, and Ag/AgCl (in saturated KCl (aq)) as a reference electrode. The transient photocurrent response for $TiO_2$ stacks in the air was recorded on an electrochemical analyzer (Auto-lab M240) at the operation voltage of 0.5 V with point light as a light source. The photoluminescence emission spectra (PL) of samples were analyzed on a fluorescence spectrophotometer (Hitachi, Model F-7000) with an excitation wavelength of 375 nm at room temperature.

### 2.3. Catalytic performances

The experiment of evaluating $CO_2$ methanation was carried in a fixed bed flow reactor under one atmospheric pressure. And a flat-plate quartz cell (30 × 20 × 0.5 mm) as the reactor with 300 mg catalyst sample (the free space was filled with silica sand) was heated by an electric resistance board.

In the typical reaction, the catalyst sample (300 mg) with a grain size of 0.2-0.3 mm was packed in a flat-plate quartz cell (30 × 20 × 0.5 mm), and heated by an electric resistance board. The temperature of the catalyst bed was monitored by a K-type thermocouple inserted into the reactor. During the photo-thermal reaction process, Xe light was irradiated form the top surface of the quartz cell. For the thermal reactions (without light), the quartz cell was enclosed by Al foils to rule out light irradiations. Before reaction, the catalyst was reduced at 320 °C for 3 h in the stream of 12.0 vol% $H_2$-He with the flow rate of 30.0 mL·min$^{-1}$. Then, the $H_2$ stream was switched to He stream, until the temperature was cooled down to room temperature. Then feed stream was immersed into water to bring vapor at a total flow rate of 60.0 mL·min$^{-1}$. After 1 h, the fed gas tune to 5.0 mL·min$^{-1}$, and outlet stream was analyzed using an online gas chromatograph (Aglient 4890D, TDX-01) equipped with a thermal conductivity detector (TCD) and a flame ionization detector (FID). During the heated reaction process, enclosed with Al foils when testing the activity of the catalyst in dark, and introduced light into the surface of the quartz cell when testing the activity of catalyst under UV-illumination. The detail

information as following:

The yield of $CH_4$ could be calculated by the equation as reference [24]:

$$Y = \frac{S_a}{S_{st} \times V \times m_{car} \times t} \quad (1)$$

Where Y was the yield of $CH_4$, $S_a$ was the area of $CH_4$ content by determining GC, $S_{st}$ was the standard $CH_4$ content with internal standard method, V was the standard molar volume, $m_{cat}$ was the mass of catalyst and t was the reaction time. Considering that the outlet gas was collected by a 1 mL quantitative ring as flowing system, the real $CH_4$ content should be multiplied flow velocity, denoted as $\mu mol \cdot g^{-1} h^{-1}$

### 2.4. Chemisorption of CO, $CO_2$ & $H_2O$

The chemisorption for CO, $CO_2$ and $H_2O$ on catalyst was respectively measured in a transform infrared spectrum (FT-IR) instrument (ThermoFisher, is-50) with Harrick in-situ heater and gas system, which contains controllable environmental chamber with two ZnSe windows interval of 120° and another mounter a quartz window. As-prepared sample was mounted into the chamber. Before the measurement, the sample was inlet mixed $H_2$-He gas at 320 °C for 1 h. After cooling to room temperature, the absorption spectrum of sample was recorded as a reference. Then, a 5.0 mL gas ($CO_2$, CO or $H_2O/CO_2$ mixed) was inlet into the chamber under the same controlled pressure. And every temperature as the catalytic performance tests were conducted, all background files using the blank atmosphere.

### 2.5. Temperature programmed surface reaction (TPSR)

For TPSR process, the sample was pretreated in 10 vol% $H_2$-Ar stream at 320 °C for 1 h, then the process of sample was proceeded as follows: (1) Introducing purity $CO_2$ (30.0 $mL \cdot min^{-1}$) into the sample for 30 min at room temperature, (2) Switching He stream till the signals of TCD and Mass signals was stable, (3) a stream of (30.0 $mL \cdot min^{-1}$) was passed through the sample with a temperature-rising rate of 10 °C $min^{-1}$ from 50 to 350 °C. Meanwhile, the mass spectrometry (MS) analysis was tell the desorption species in contents of $CH_4$, $H_2O$, CO, $CO_2$ et al. Here, the He carrier was applied to monitor C-containing products, Ar carrier was applied to monitor H-containing products.

## 3. Results & discussion

### 3.1. Characterizations of catalysts

As expected, $TiO_2$ sample was prepared by hydrothermal strategy as confirmed by X-Ray diffraction (XRD) patterns (Fig. 1a). All patterns could be well indexed to anatase structure corresponding to the JCDPS no.01-071-1166. Diffraction peaks at 2θ values of 25.30, 37.80, 48.04, 53.98, 56.06, 62.69, 68.76 and 75.06 could be assigned to the (1 0 1), (0 0 4), (2 0 0), (1 0 5), (2 1 1), (2 0 4), (1 1 6), and (2 1 5) crystallographic planes of the anatase $TiO_2$. The phase information was further verified by UV Raman spectroscopy (excitation at 325 nm, seeing Fig. S1 in SI). None of characteristic Cu peaks were detected in XRD, indicating that Cu was highly dispersed on the surface of support with extremely small Cu clusters or low concentration [19]. Meanwhile, characteristic peak of CDs (*c.a.* 26°) was not detected in the patterns, which might be attributed to the low content and high dispersion of the CDs [36]. Note that the crystalline size of $TiO_2$ would be enlarged by introducing Cu species and CDs (seeing Table S2 in SI). Here, the crystalline size of $TiO_2$ (calculated by Scherrer equation) was 11, 26 and 24 nm in $TiO_2$, $Cu/TiO_2$ and $Cu/TiO_2$-C sample, respectively.

The light absorption capability of samples was determined by UV–vis diffuse reflectance spectra (DRS, Fig. 1b). $Cu/TiO_2$ sample was exhibited a light absorption at 420 nm (band gap is 2.95 eV) [37]. However, the intrinsic light absorption of $TiO_2$ (band gap is 3.2 eV) was found about 380 nm [38], this reason could be attributed to the redistribution of $TiO_2$ electrical charge by Cu modification [39]. In fact, all samples were still exhibited the UV absorption whatever CDs was present or absent, suggesting the negligible changes by adding CDs. Notably, a broaden adsorption band above 600 nm could be attribute to the d-d transition of Cu ions (Fig. 1b, insert) [40].

The nanostructure of the $Cu/TiO_2$-C sample was demonstrated by TEM as revealed in Fig. 2. Clearly lattice spacing of $TiO_2$ (~0.35 nm) and CDs (~0.33) lattice were observed by the high resolution TEM (HRTEM) in Fig. 2a, corresponding to the plane of $TiO_2$ (1 0 1) and CDs (0 0 2) [41,36]. Moreover, a certain amorphous cycle was exhibited in the SAED image of Fig. 2b, which could be attributed to the amorphous CDs nanoparticles [35]. Individual Cu particles were not found by the HRTEM images, which may be attributed to low concentration of Cu loading, consistent to the result of XRD. However, Cu species was demonstrated by EDX spectrum (Fig. 2c), suggesting the presence of Cu specie. The mapping result (Fig. 2d) further suggested that the Cu species were dispersed on $TiO_2$, homogeneously. In addition, TEM also showed that all of $TiO_2$, $Cu/TiO_2$ and $Cu/TiO_2$-C consisted of irregular sphere-shaped, the $TiO_2$ crystalline particle size in $TiO_2$, $Cu/TiO_2$ and $Cu/TiO_2$-C was around 12.78, 24.84 and 21.49 nm, respectively (seeing Fig. S2 in SI), in good agreement with XRD results.

Additionally, the textual property of $TiO_2$ was unchanged by introduction of CDs or Cu. The results of $N_2$ adsorption-desorption experiments of samples (seeing Fig. S1 in the supporting information (SI)) indicated all samples were exhibited the IV type of nitrogen isothermal stripping curves [42]. Meanwhile, there were slightly changed in surface area, pore diameter and pore volume after depositing Cu or CDs (seeing Table S2 in SI).

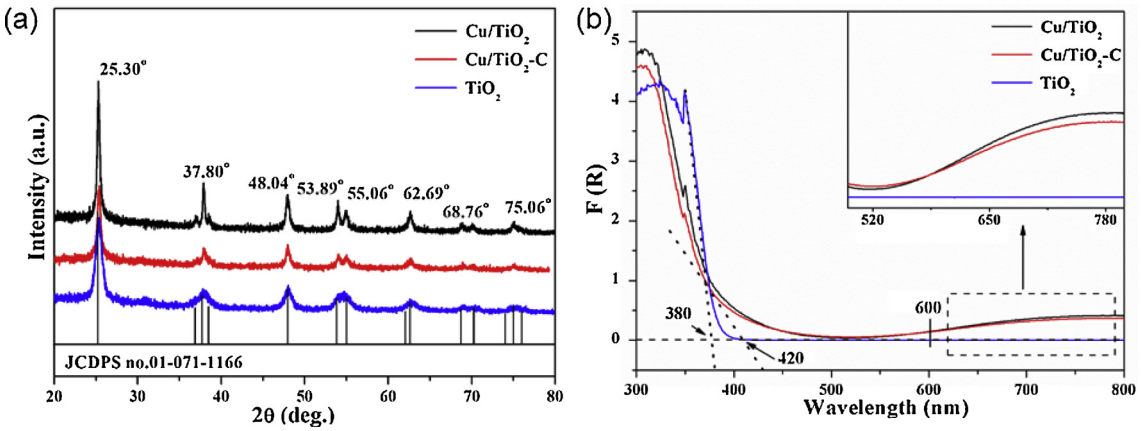


**Fig. 1.** (a) X-Ray diffraction patterns and (b) UV–vis diffuse reflectance spectra of $Cu/TiO_2$, $Cu/TiO_2$-C and $TiO_2$ sample.

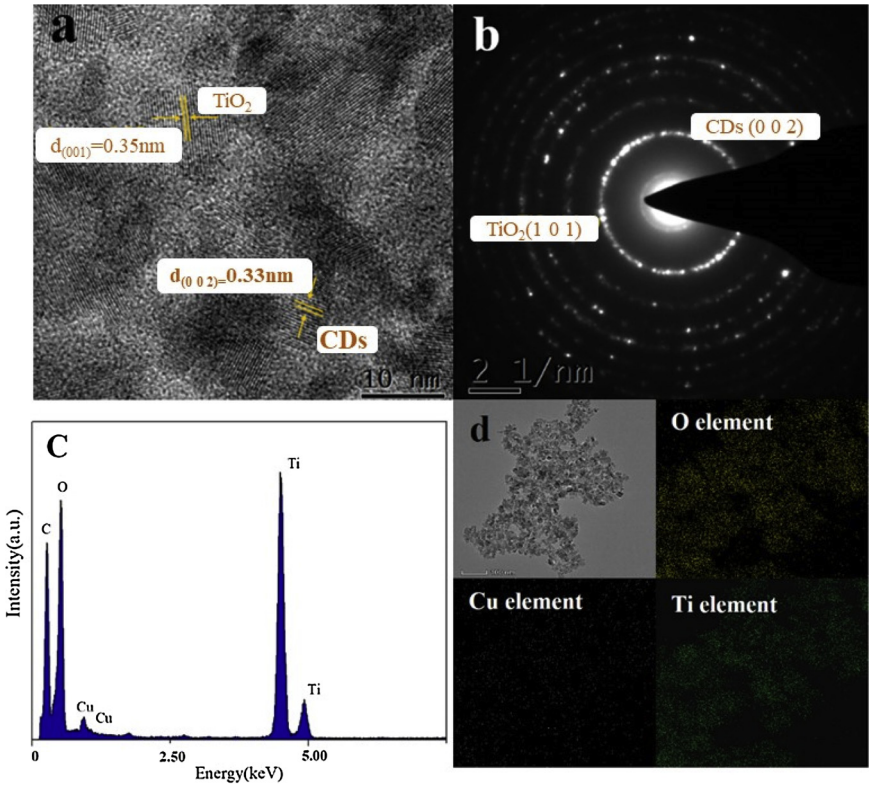


**Fig. 2.** High resolution TEM image (a), SAED pattern (b), EDX spectrum (c) and TEM-EDX mapping (d) of $Cu/TiO_2$-C sample.

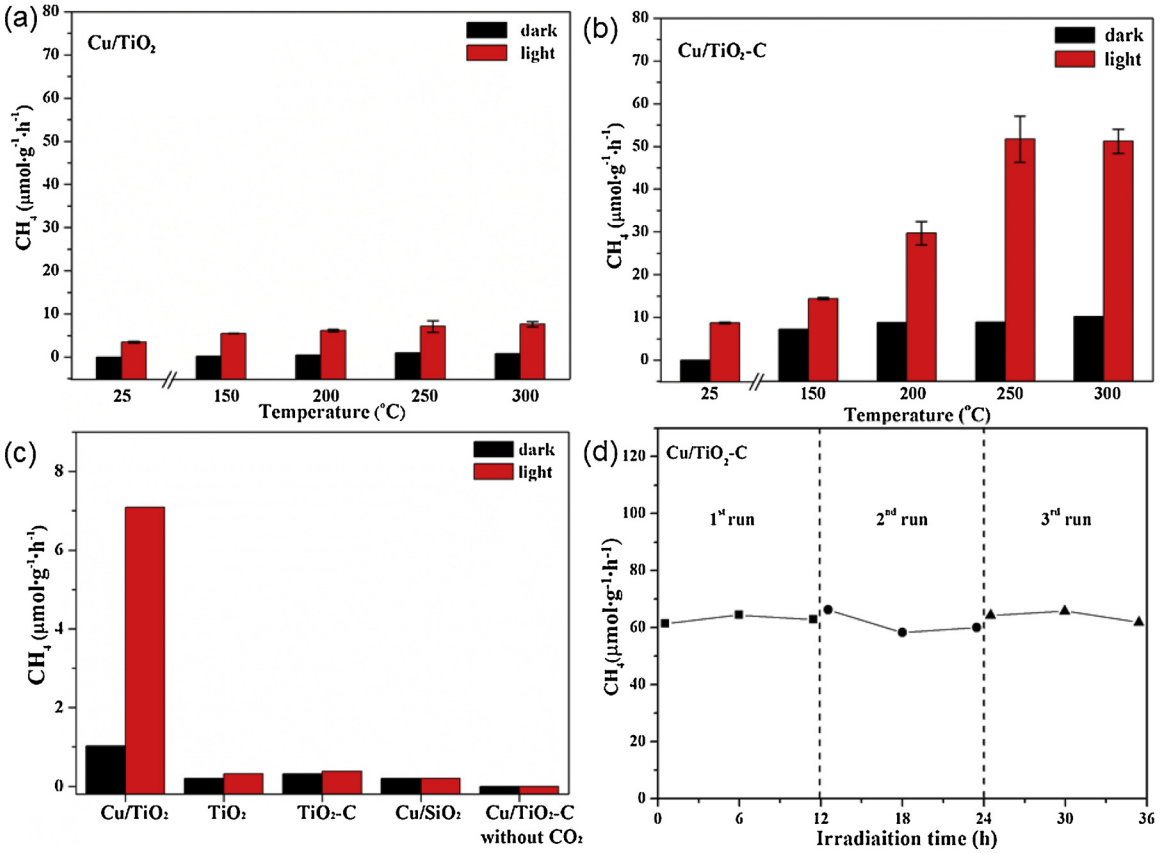


**Fig. 3.** The catalytic performances of (a) $Cu/TiO_2$, (b) $Cu/TiO_2$-C and (c) various samples for $CO_2 + H_2O$ reaction at different temperature under UV-irradiation or in dark; and (d) stability over $Cu/TiO_2$-C under UV-irradiation.

### 3.2. Catalytic performances

Fig. 3 shows the catalytic performance of $Cu/TiO_2$ and $Cu/TiO_2$-C samples for $CO_2$ + $H_2O$ reaction at various temperatures under UV irradiation or not. It was found that almost no $CH_4$ was produced in the $Cu/TiO_2$ sample (Fig. 3a) at each temperature under dark, but the trace yield of $CH_4$ was appeared under UV irradiation. Here, highest methanation activity is about 8 μmol $g^{-1}$ $h^{-1}$ at 250 °C under UV irradiation. For the $Cu/TiO_2$-C sample (Fig. 3b), none of $CH_4$ was detected at low temperature (< 150 °C) under dark, but $CH_4$ was slightly increased with temperature up (> 150 °C). Furthermore, $CH_4$ activity was stable from 150 to 300 °C under dark, indicating that a simply increase of temperature did not enhance the reaction proceeding. By introducing UV light, the $CH_4$ production was dramatically increased, especially at a high temperature (the highest value is 60 μmol $g^{-1}$ $h^{-1}$ at 250 °C). Note that the $CH_4$ production at 25~125 °C with UV irradiation was almost equal to that at a high temperature without UV irradiation, indicating that the activity of $CH_4$ in $Cu/TiO_2$-C sample would not be enhanced by single increasing temperature or introducing UV light. In other words, the photo-assistant effect for the reaction of $CO_2$ + $H_2O$ only occurred on $Cu/TiO_2$-C by increasing temperature. This result also demonstrated that the introduction of CDs into $Cu/TiO_2$ not only promoted the thermal-catalytic activity of $CO_2$ methanation, but also dramatically promoted the photo-thermal catalytic activity. In fact, the 1.0 wt% Cu content of the as-prepared $Cu/TiO_2$-C sample was an optimal value of Cu loading (seeing Fig. S2 in SI). However, the catalytic performance in this work is hard to compare with the reported results about $CO_2$ photoreduction over Cu or CDs catalysts [19,43–45], because the reaction system (a fixed bed flow reactor at high temperature and UV irradiation) is different from the reports.

Notably, a few of $CH_4$ was observed in pure $TiO_2$ or $TiO_2$-C sample under the dark condition (Fig. 3c), indicating that the formation of $CH_4$ would be promoted by modifying Cu into $TiO_2$ or $TiO_2$-C [1,2]. Here, the active sites were formed by Cu species for $CO_2$ adsorption and conversion and charge separation of $TiO_2$ [24,25]. Although a trace of $CH_4$ was detected under dark at 250 °C in non-semiconductor sample ($Cu/SiO_2$), $CH_4$ activity was unchanged under UV irradiation. These results indicated that the photo-assistant effect of $CO_2$ methanation in $TiO_2$ or $TiO_2$-C samples was actually originated from $TiO_2$ photo-excitation. In addition, none of $CH_4$ product was detected over $Cu/TiO_2$-C sample without $CO_2$ gas, indicating that the formed $CH_4$ was mainly resulted from $CO_2$ not the C residual in the sample. In addition, the isotopic labeling experiment, conducted by GC–MS with $^{13}CO_2$ reactants, showed that the $^{13}CH_4$ with $m/z$ = 17 was the main product (seeing Fig. S5 in SI), suggesting that the $CH_4$ was produced from reduction of $CO_2$. As can be seen, the co-operation effect of Cu, CDs and $TiO_2$ could be responsible for $CO_2$ methanation by $H_2O$ at a high temperature under UV-irradiation. Moreover, this synergetic effect showed a good stability after three cycling experiments (Fig. 3d). Interestingly, the trace of $H_2$ was detected by MS (seeing Fig. S6 in SI), indicating that $H_2$ would be produced during the reaction. This $H_2$ formation would be further discussed in the section of 3.6.2.

### 3.3. XPS results (Element surface states)

Considering that the elemental states has a dramatic influence to the catalytic performance, the high-resolution XPS were carefully investigated to determine the surface composition and oxidation states of all samples after different treatments. As can be seen from the XPS profile of C1 s of $Cu/TiO_2$-C and $Cu/TiO_2$ samples in Fig. 4a and b, an obviously characteristic peak of O-C = O species (~292.70 eV) was observed in the $Cu/TiO_2$-C sample, indicating the existence of CDs species [46]. Although, the peak of O—C═O species was shifted negatively to the direction of lower binding energy about 0.3 eV after $H_2$ treatment (curve B in Fig.4 a), this peak was backed to the original position after $CO_2$ + $H_2O$ reaction (curve C in Fig.4a). This indicated that the CDs could store electrons and release these electrons during the reaction proceedings, thus an excellent separation of charges under UV irradiation. Additionally, three peaks of graphite carbon (~284.60 eV), C-O (H) (~286.40 eV) and C═O (~288.70 eV) species were deconvoluted in the $Cu/TiO_2$-C and $Cu/TiO_2$ samples, respectively [46]. Except that the increased of C-O(H) species was demonstrated in $Cu/TiO_2$-C sample after $H_2$ treating, other peaks were negligible changed in $Cu/TiO_2$-C and $Cu/TiO_2$ sample after different treatments.

Fig. 4c and 4d show the Cu 2p XPS profile of $Cu/TiO_2$-C and $Cu/TiO_2$ samples. Where the Cu (I) $2p_{3/2}$ and Cu (I) $2_{1/2}$ spin-orbital splitting photoelectrons was found at 932.80 and 952.55 eV [47]. It was apparently found that a stable Cu (I) species was exhibited over $Cu/TiO_2$-C after various treatments (Fig. 4c). Interestingly, the BE value of Cu (I) in the $Cu/TiO_2$ sample was determined at the original location even after $H_2$ treating (curve B in Fig. 4c), but a negative shift BE value (from 933.10–933.00 eV) was illustrated after $CO_2$ + $H_2O$ reaction. This result further indicated that CDs could act an electrons reservoir to store and release electrons during the $CO_2$ + $H_2O$ reaction. With respect to the Cu states in the $Cu/TiO_2$ sample (Fig. 4d), diversified oxidation states of Cu species were discovered after various treating. Initially, the peaks of Cu (0) $2p_{3/2}$ and Cu (II) $2p_{3/2}$ were found (curve A in Fig. 4d) at 932.05 and 934.40 [48], then the increased of Cu (0) species was exhibited after $H_2$ treating, finally the Cu(II) species was formed as mainly species after $H_2O$ + $CO_2$. Maybe, a stable Cu (I) species could be responsible for the higher catalytic activity of $Cu/TiO_2$-C sample. In that case, an electrons storage was formed by adding CDs to separate charges efficiently. In addition, the Ti 2p and O 1s profile of the above two samples were also tested after same treatments (seeing Fig. S3 in SI). Here, a negligible changed of Ti species was shown in the $Cu/TiO_2$-C and $Cu/TiO_2$ sample. However, the higher BE value of O1 s was demonstrated in the $Cu/TiO_2$-C as compared to $Cu/TiO_2$ sample, indicating the interaction between $TiO_2$ and CDs (Fig. S3).

### 3.4. Photocurrent & photoluminescence results

The photocurrent responses were evaluated with three electrode cell to investigate the charge generation and recombination in $Cu/TiO_2$ and $Cu/TiO_2$-C samples in Fig. 5a. As can be seen, the $Cu/TiO_2$-C sample exhibited an obviously photocurrent as compared to $Cu/TiO_2$, indicating that an excellent charge separation occurred by introducing of CDs. Moreover, the PL changes was observed in different samples further providing an information for the efficient charge transfer. Fig. 5b shows the PL emission signal of $Cu/TiO_2$-C and $Cu/TiO_2$ sample by using 380 nm excitation light. A weaker emission signal at 568 nm could be assigned to the emission of $TiO_2$ [49] was exhibited in the $Cu/TiO_2$-C sample as compared to $Cu/TiO_2$, indicating the efficient charges separation with presence of CDs. In addition, an apparently peak at 443 nm in the $Cu/TiO_2$-C could be attribute to the emission of CDs [35]. Both the photocurrent and PL results showed that the photo-excited electrons could be separated by adding CDs. In this case, the reaction could be enhanced under UV irradiation by the rich surface electrons of $Cu/TiO_2$-C (seeing XPS result in Fig.4).

### 3.5. In-situ DRIFTS of samples for $CO_2$ + $H_2O$

To investigate $CO_2$ transformation, the in-situ DRIFTS were conducted to simulate $CO_2$ + $H_2O$ reaction in various temperature under UV irradiation or not. Fig. 6a shows the IR diffraction of $Cu/TiO_2$-C sample in $CO_2$ + $H_2O$ atmosphere at 50 °C, no peaks were observed at lower wavenumber (< 1600 $cm^{-1}$) after adsorbing $CO_2$, indicating that $CO_2$ intermediates was hardly formed in this temperature. However, the obviously peak at 1620 $cm^{-1}$ could be attributed to the hydroxyls (H-O-) bending mode, especially for isolated hydroxyls molecules [50]. When the UV light was introduced, the H-O- peak was increased and another peak was emerged at 1420 $cm^{-1}$, which ascribed to the carbonate ($*CO_3^{2-}$) species [51], suggesting the adsorption of $CO_2$ could be

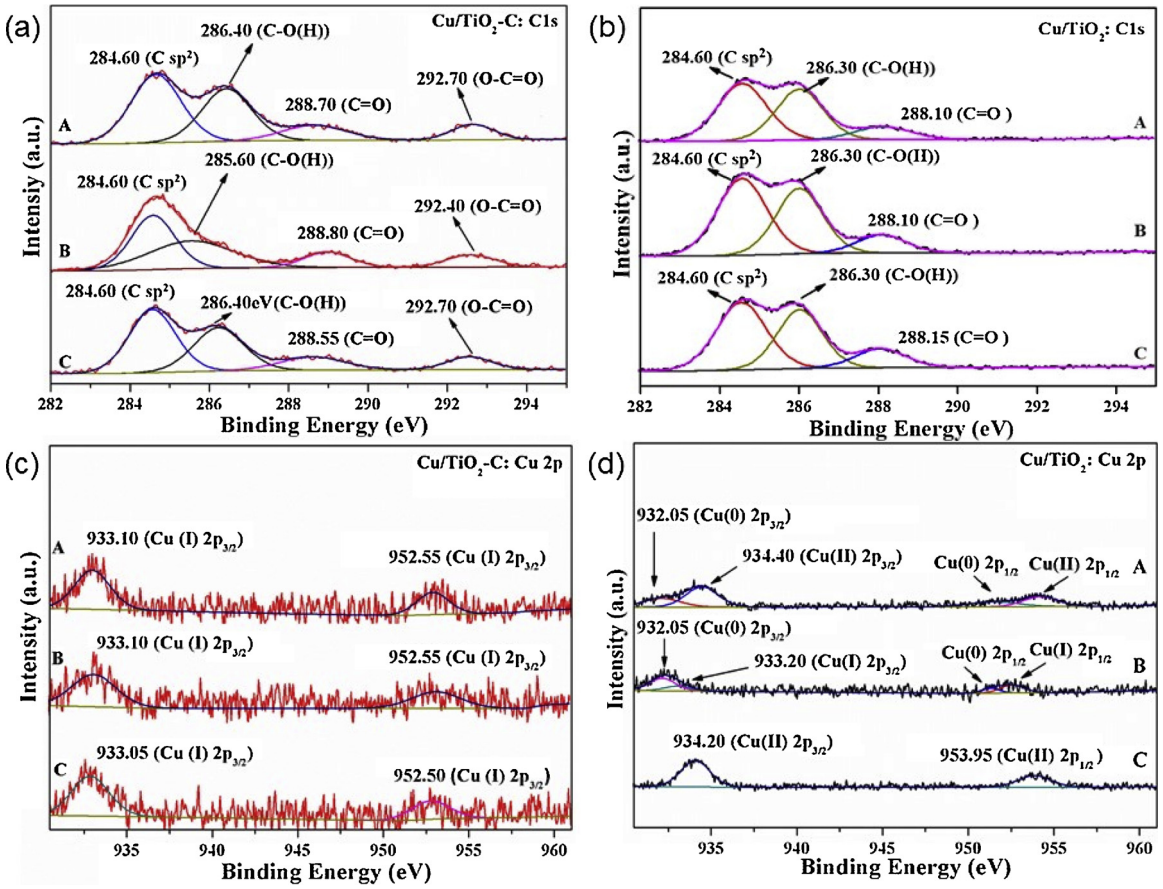


**Fig. 4.** The respective high-resolution XPS profile of C 1s (a, c) and Cu 2p (b, d) of $Cu/TiO_2$-C and $Cu/TiO_2$ samples, after different treatments: A: fresh sample, B: after $H_2$ reduction at 320 °C for 3 h, C: after reaction of $CO_2$ + $H_2O$ under 250 °C under UV illumination for 5 h.

promoted by introducing UV irradiation. The results demonstrated that a poor $CO_2$ activity in the lower temperature could be attributed to a weak $CO_2$ adsorption. While temperature increasing to 150 °C, an obviously $*CO_3^{2-}$ peak was exhibited even under dark (Fig. 6b), further indicating that the adsorption of $CO_2$ would be enhanced with a rise of temperature. Furthermore, the $*CO_3^{2-}$ and H-O- peaks were increased under UV irradiation, suggesting the promotion of $CO_2$ and $H_2O$ adsorption in that condition. When temperature up to the 200 °C (Fig. 6c), the OCO stretching of the bridging formate species (*HCOO species) was revealed at 1558 $cm^{-1}$ [52,53] both in dark or UV irradiation. Meanwhile, a sharply CO species (*CO) peak was recorded at 2118 $cm^{-1}$, which was always deemed as the species of adsorbed CO on Cu [54,55]. After introducing UV light, the *CO species was decreased, indicating that CO species could be further transformed after UV irradiation. When temperature at 250 °C (Fig. 6d), *HCOO and H-O- species were observed under dark, however, *HCOO and H-O- species was decreased under UV irradiation after 10 min. Considering that the best $CH_4$ activity in the reaction occurred at 250 °C under UV irradiation (seeing Fig. 3); therefore, it was easily proposed that *HCOO species would act as intermediate to form $CH_4$ during the reaction. Note that the no obviously *CO species was monitored in 250 °C, suggesting that *CO would be another intermediate to form $CH_4$. Comparing the process of $CO_2$ + $H_2O$ in $Cu/TiO_2$ sample, the same operations were carried out in different temperature.

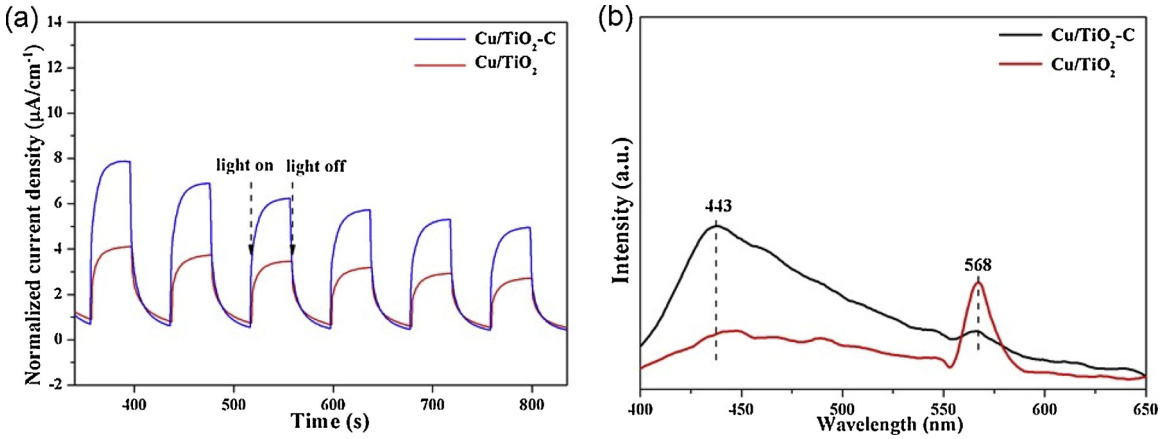


**Fig. 5.** Transient photocurrent responses (a) and photoluminescence results (b) of the $TiO_2$, $Cu/TiO_2$ and $Cu/TiO_2$-C samples.

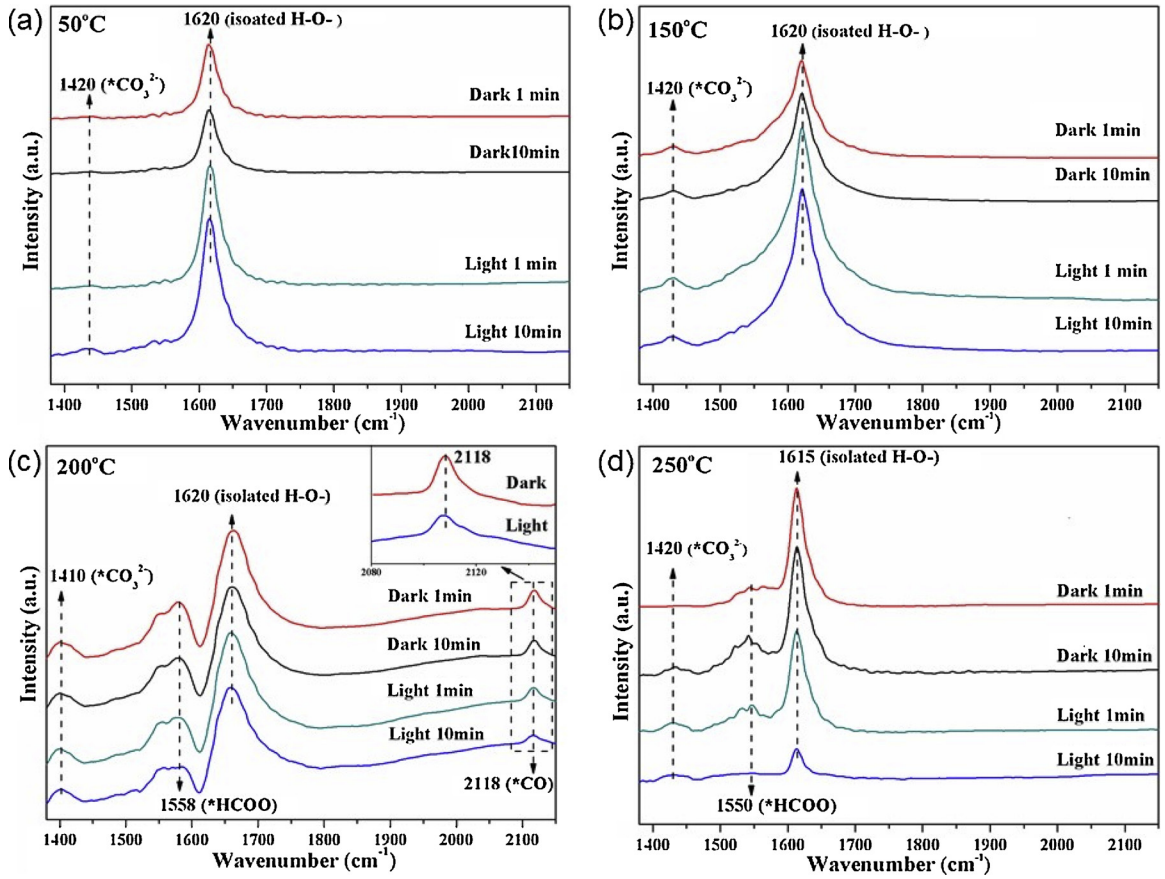


**Fig. 6.** In-situ DRIFTS of Cu/$TiO_2$-C sample at 50 °C (a), 150 °C (b), 200 °C (c) and 250 °C (d) with $CO_2$ + $H_2O$ gas inlet.

Fig. 7a reveals the IR diffraction of Cu/$TiO_2$ at 50 °C, a weak $H_2O$ adsorption was exhibited in Cu/$TiO_2$, compared with Cu/$TiO_2$-C. It meant that the adsorption of $H_2O$ could be promoted by modifying the CDs. With the rising of temperature (Fig. 7b-d), a sort of irregular multi-carbonate peaks was appeared at 1397 $cm^{-1}$ [41], and these peaks would be enhanced after UV irradiation, in good agreement with the results of Cu/$TiO_2$-C sample. However, the poor adsorption of $H_2O$ (weak peak at ~1620 $cm^{-1}$) was always observed in Cu/$TiO_2$ sample at various temperature, indicating a worse $H_2O$ adsorption without CDs. Notably, a tiny *CO species was recorded in Cu/$TiO_2$ at 250 °C, however, the *CO formed temperature was shifted to lower in Cu/$TiO_2$-C sample (200 °C). According to the result of XPS, a stable Cu (I) was presented in the Cu/$TiO_2$-C, therefore, it was deduced that the excellent activity of Cu/$TiO_2$-C could be attributed to a feasible *CO species with presence of Cu (I) ($CO_2$ + $Cu_2O$ → CO + CuO). Furthermore, $CO_2$ adsorption experiments were measured at 273 K to examine the capability of adsorbing $CO_2$ (physical adsorption). As compared Cu/$TiO_2$ samples, the Cu/$TiO_2$-C sample exhibited a much higher adsorption quantity (seeing Fig. S4 in SI). By normalizing with respect to surface area, it can be calculated that the $CO_2$ adsorption quantity of sample was not caused by the change of its specific surface (Table S2 in SI). This result further showed that the capability of adsorbed $CO_2$ could be promoted by introducing the CDs.

### 3.6. TPSR testing of Cu/$TiO_2$-C sample

#### 3.6.1. TPSR of $CO_2$ + $H_2O$

Although the rich information of reactants adsorption was obtained from the in-situ DRIFTS, some species were not monitored, especially for $CH_4$ species due to an insensitivity of trace $CH_4$. So, the TPSR-MS tests of Cu/$TiO_2$-C sample were carried out in Fig. 8. Where $H_2O$, as the major desorption species, would be desorbed at 200 and 310 °C in dark (Fig. 8a), and $CO_2$ was exhibited at 80 °C, indicating a strong adsorption of $CO_2$ and $H_2O$ species at sample, in great agreement with the results of the in-situ DRIFTS. A trace of CO species would be desorbed at 125 and 215 °C, while a trace of $CH_4$ was produced at start of 130 °C. This result demonstrated that the production of $CH_4$ might be originated from CO species. Zhu et al. pointed out that the water-gas shift reaction (WSG, CO + $H_2O$ → $CO_2$ + $H_2$) usually occurred in a high temperature, especially in presence of Cu type catalysts [56]. Subsequently, the formed $H_2$ by WGS would be further reacted with CO to produce $CH_4$.

After UV irradiation, $H_2O$ would be desorbed at 200 and 300 °C with a larger peak (Fig. 8b), indicating that the desorption of water could be promoted by UV irradiation, consistent with the result of in-situ DRIFTS. Compared with dark, CO would be desorbed peak at a lower temperature (110 and 185 °C) after UV irradiation, suggesting the presence of feasible CO intermediate under UV irradiation. Furthermore, another peak of $CH_4$ was also exhibited at 190 °C, further indicating that the formation of $CH_4$ could be enhanced by the presence of CO. As can be seen, the process of $CO_2$ methanation by $H_2O$ over Cu/$TiO_2$-C sample may be accompanied by the WGS reaction (producing $H_2$).

#### 3.6.2. TPSR of $CO_2$ + $D_2O$ (isotope label experiments)

To confirm the above assumption, the isotopic label experiments were conducted with water/deuterium agent to verify the resource of hydrogen. Before the operation, the He carrier was changed by Ar carrier due to a higher sensitive of H-containing species, especially for $H_2$ and $D_2$. As revealed in Fig. 9a, the $H_2$ peak was mainly observed at 110 °C under dark, indicating that $H_2$ would be produced by CO + $H_2O$ reaction (WGS) with a higher CO desorbed temperature (120 °C, seeing Fig. 8a). However, the $D_2$ species was hardly formed in this condition, which could be attributed to a weak adsorption of $D_2O$ species (desorbed temperature at 70 °C). After adsorbing $CO_2$ under UV irradiation

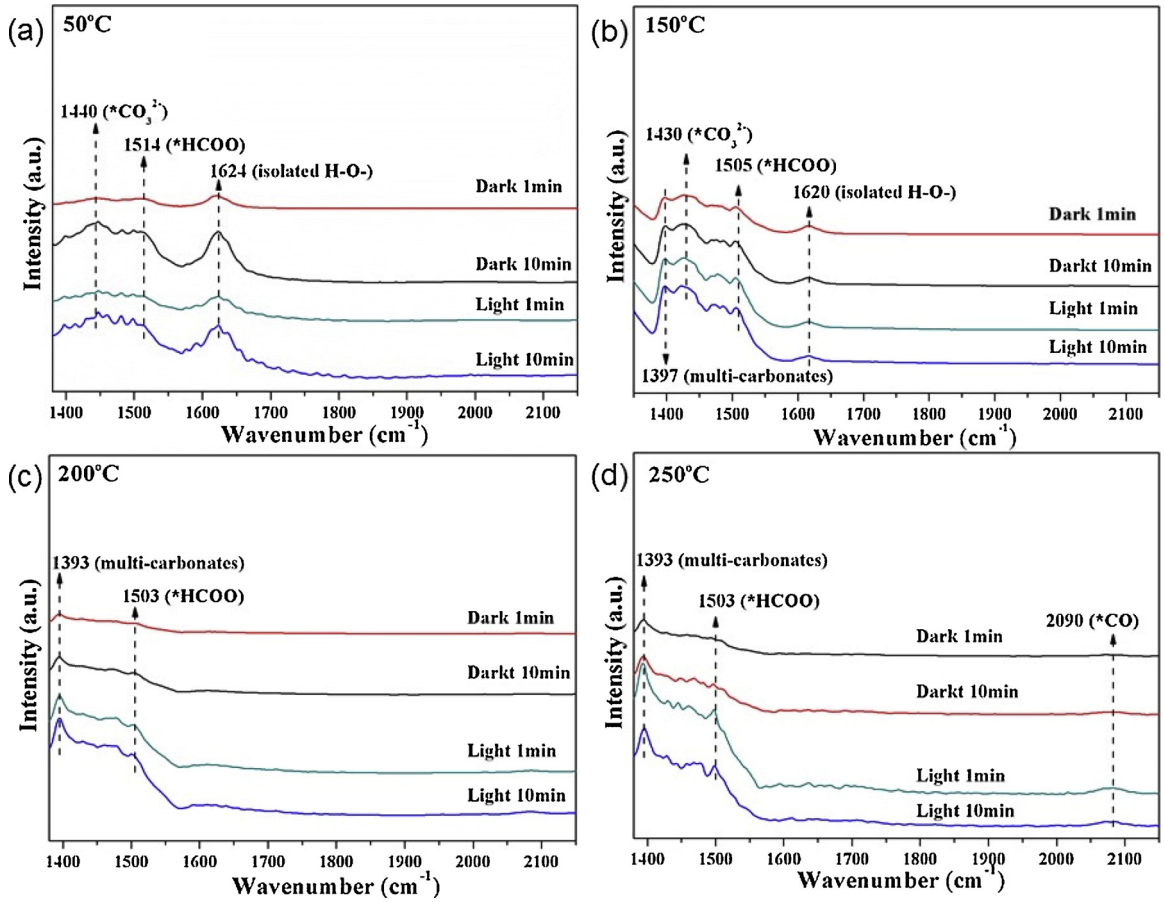


**Fig. 7.** In-situ DRIFTS of $Cu/TiO_2$ sample at 50 °C (a), 150 °C (b), 200 °C (c) and 250 °C (d) with $CO_2$ + $H_2O$ gas inlet.

(Fig. 8b), three $H_2$ peaks appeared at 170, 250 and 350 °C, indicating that more $H_2$ would be produced after UV irradiation. In this time, it was found that some $D_2$ peaks were detected (160 and 260 °C). Results demonstrated that the promotion of $D_2$ could be ascribed to the promotion of $D_2O$ adsorption (desorption at 115 °C) and the facilitated CO formation (desorption at 110 °C). Meanwhile, $CH_4$ ($m/z$ = 16) and $CH_3D$ ($m/z$ = 17) species were detected in MS (Fig. 9), indicating that the activity of $CH_4$ could be promoted by forming $H_2$. The result confirmed the above assumption that WGS reaction would be enhanced under UV irradiation with a favorable of CO formation. Interestingly, there was different desorption temperature for water and deuteroxide, the desorbed temperature of $D_2O$ was lower than that of $H_2O$. The result could be attribute to the different hydrogen bond mode in $H_2O$ and $D_2O$. [57]

### 3.6.3. In-situ DRIFT of WGS reaction over $Cu/TiO_2$-C

The in-situ DRIFTS tests were carried out by using CO and vapor continuous gas flow with higher CO concentration (5 vol%) to monitor the detail of WGS process, as revealed in Fig. 10. After introducing of mixed gas, three apparent peaks could be observed (curve A), of which two peaks at 2110 and 2170 $cm^{-1}$ could be attributed to the CO gaseous species, and the peak at 2350 $cm^{-1}$ attributed to the gaseous $CO_2$, respectively [58]. In addition, two peaks at 2900 and 2950 $cm^{-1}$ was recorded, indicating that $CH_x$ was formed as $CH_4$ intermediate [59,60].

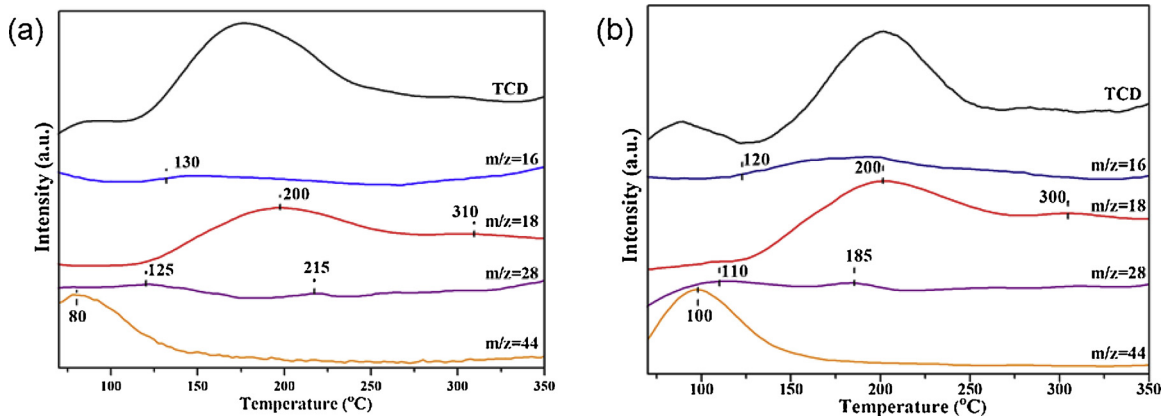


**Fig. 8.** The temperature programmed surface reaction mass spectrometry of $CO_2$ + $H_2O$ over $Cu/TiO_2$-C sample under dark (a) and light (b) condition. Mass signals of $m/z$ = 16, 18, 28 and 44, referencing to methane ($CH_4$), water ($H_2O$), carbon monoxide (CO) and carbon dioxide ($CO_2$), respectively.

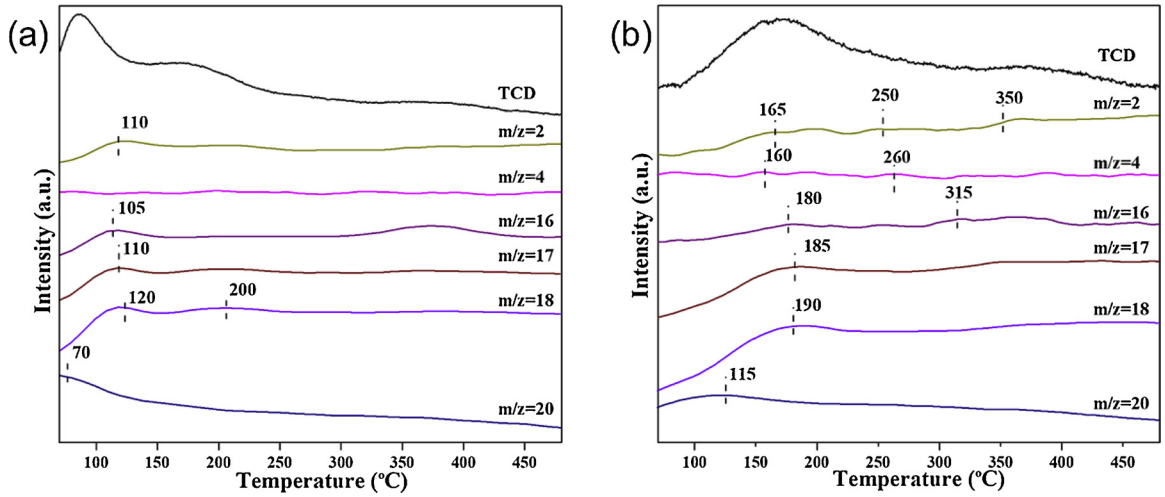


**Fig. 9.** The temperature programmed surface reaction mass spectrometry of $CO_2 + D_2O$ over $Cu/TiO_2$-C sample under dark (a) and light (b) condition. Mass signals of $m/z$ = 2, 4, 1618 and 20, referencing to $H_2$, $D_2$, $H_2O$ and $D_2O$, respectively.

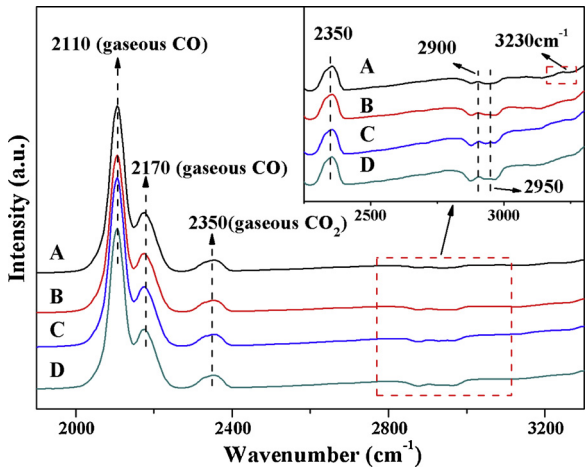


**Fig. 10.** In-situ DRIFTS of $Cu/TiO_2$-C at 200 °C with $CO + H_2O$ gas inlet in dark 1 min(A), 10 min(B) and UV irradiation 1 min (C), 10 min(D).

Notably, a tiny peak at 3230 $cm^{-1}$ could be found in the first place (curve A in Fig. 10), suggesting that the adsorbed $H_2$ on Cu (Cu-$H_2$) species [61]. The result also revealed that $H_2$ would be produced from WGS process under the dark condition. After UV irradiation, the $CH_x$ species was increased and Cu-$H_2$ decreased, indicating the promotion of WGS proceeding and therefore conversion of $CH_4$.

### 3.7. In-situ DRIFTS for proton hydrogen from $H_2O$ splitting

According to the many reports, the protons would be produced under UV irradiation via $H_2O$ splitting [24]. Another process might occur by introducing UV light, that could be through $H_2O$ dissociation to protons, then it reacted with *HCOO to form $CH_4$ [24]. To verify this proposition, a static in-situ DRIFTS experiments was conducted in $Cu/TiO_2$-C sample to investigate the water behavior.

As reveal in Fig. 11a, peaks at 1250, 1410 and 1640 $cm^{-1}$ after adsorbing $H_2O$ in $Cu/TiO_2$ could be assigned to the multi-carbonates, $H_2O$ and carbonates species, respectively [8,41,50]. After UV irradiation, a small peak at 1480 $cm^{-1}$ (Fig. 11a, curve Light and L−D) could be attributed to the adsorbed proton on Cu sites ($CuH_2$-) [62], suggesting the presence of protons through $H_2O$ splitting. That is to say, $CH_4$ might be formed by hydrogenation of $CO_2$ using these protons. The isotopic label testing for $Cu/TiO_2$-C sample was also carried out by deuterium oxide ($D_2O$) agent in Fig. 11b. It was obvious that none of $H_2O$ peak (~1620 $cm^{-1}$) was observed, but a weak OD band vibration was appeared at 2200 $cm^{-1}$, indicating the presence of adsorbed $D_2O$ species. After UV irradiation, a new peak at 1580 $cm^{-1}$ (Fig. 11b, curve Light and L−D) could be attributed to the particular deuterohydrogen bonded on the Cu species (CuHD-) [61]. This meant that the formed protons species on $Cu/TiO_2$-C should be originated from the injected $H_2O$, and enhanced the hydrogenation of $CO_2$ under UV irradiation. Notably, the adsorption of $D_2O$ was promoted by UV irradiation, confirming the result in TPSR (Fig. 9).

### 3.8. A proposed reaction mechanism

Based on above results, it is proposed that the $CO_2$ methanation process over $Cu/TiO_2$-C above 150 °C under UV irradiation could be regarded as the cycle of two main processes: One is the $CO_2$ methanation induced by $Cu_2O$ above 150 °C in dark, and the other is in-situ regeneration of $Cu_2O$ induced by UV light.

I. $CO_2$ methanation induced by $Cu_2O$ above 150 °C in dark:

This reaction process can be divided into two main spontaneous thermodynamic processes: $CO_2$ is firstly reduced by $Cu_2O$ to CO ($CO_2 + Cu_2O \rightarrow CO + CuO$), and then CO is reduced by $H_2O$ to $CH_4$ via water-gas shift process.

(I-a) $Cu/TiO_2$-C is treated by $H_2$ at first:

$$CuO{-}\ CDs + H2 \xrightarrow{320^{\circ}C} Cu2\ O{-}\ CDs + H2O$$

$CO_2$ is reduced by Cu(I) ($Cu_2O$) into CO: (I-b)

$$CO2 + Cu2\ O \xrightarrow{150^{\circ}C} CO + CuO$$

CO methanation by $H_2$ is produced via a WGS reaction: (I-c)

$$CO + H2\ O \xrightarrow{150^{\circ}C} \xrightarrow{Cu(II)} CO2 + H2$$

$CO_2$/CO is hydrogenated to $CH_4$ via *HCOO intermediates: (I-d)

$CO_2$/CO + Oxygen vacancies ($V_o$)→ *HCOO-Vo

*HCOO− Vo + H2 → CH4 + H2 O+ Vo

During the above processes, the $Cu_2O$ sites at catalyst surface will be consumed to suppress the continuous proceeding of $CO_2$ reduction, resulting in a lower activity in dark.

Under UV irradiation, CuO can be reduced to $Cu_2O$ again by the photo-excited electrons from $TiO_2$, the $Cu_2O$ active sites are

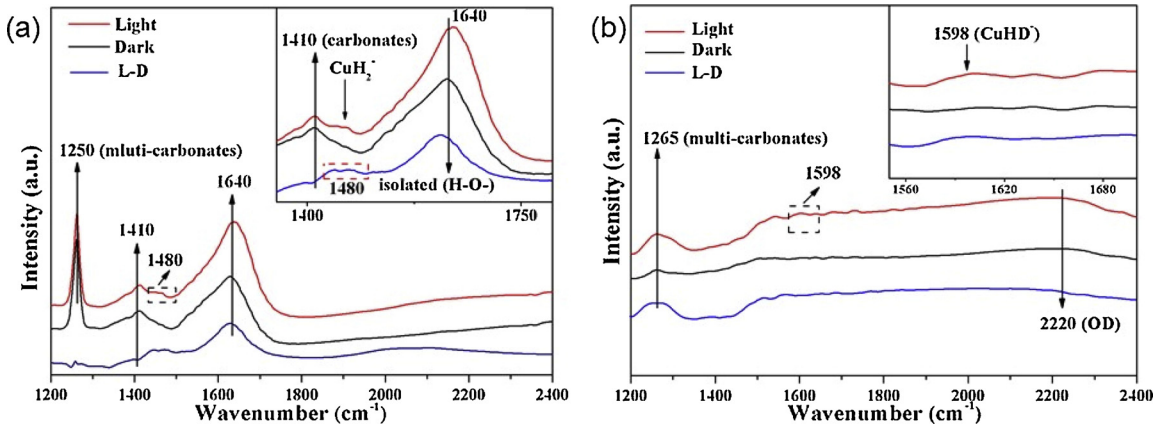


**Fig. 11.** In-situ DRIFTS specra of Cu/$TiO_2$-C sample with $H_2O$ (a) and deuterium oxide (b) in dark or under UV irradition, here, the curve L-D was obtianed by division of light and curve dark.

regenerated by the co-operation effect of $TiO_2$ and CDs. This process can be described as follows:

**II. In-situ regeneration of $Cu_2O$ under UV light:**

(II-a) $TiO_2$ is excited by UV light:

$TiO_2 \xrightarrow{hv} e^- + h^+$

(II-b) In-situ regeneration of $Cu_2O$ by reducing CuO:

$CuO + e^- \rightarrow Cu_2O + O_2$

(II-c) The electron-rich CDs captures the holes:

$CDs + h^+ \rightarrow CDs(h^+)$

Here, a little CDs may be oxidized by $O_2$:

$O_2 + CDs \rightarrow CDs\text{-}O$

During the above processes, the re-generation of $Cu_2O$ (Process II-b) can ensure the continuous proceeding of $CO_2$ methanation via Process I. This cycle of Process I and Process II is briefly described in Fig. 12. In addition, the CO produced by Process I may be also reduced by H· via $H_2O$ protonation (seeing Fig. 11) to $CH_4$ under UV irradiation (another pathway):

$H_2O \xrightarrow{e^-} H\cdot + OH^-$

$*HCOO\text{-}V_o + H\cdot \rightarrow CH_4 + V_o$

For Cu/$TiO_2$ sample, since CuO is mainly reduced to Cu(0) ($CuO + H_2 \xrightarrow{320°C} Cu + H_2O$) during the $H_2$ pretreatment process due to no CDs, $CO_2$ cannot be reduced into CO in the absence of $Cu_2O$, resulting in the non-proceeding of the subsequent reactions (Processes I-c and I-d) in dark. Moreover, UV light cannot promote the formation of $Cu_2O$, thus it does not apparently promote the proceeding of the whole reaction over Cu/$TiO_2$. However, $H_2O$ can be slightly split into the proton hydrogen under UV irradiation, resulting in the reduction of $CO_2$ by this proton hydrogen (a low activity). This may also be the reason that $TiO_2$ and $TiO_2$-C samples exhibited a little photo-assisted catalytic activity (seeing Fig. 4c). Of course, Cu/$SiO_2$ sample does not show any photo-assisted effect on this reaction, because $SiO_2$ cannot be excited by this UV light. In addition, for the very low activity of $TiO_2$ and $TiO_2$-C samples at 250 °C in dark, it can be attributed to the effect of the hydrogen stored at $TiO_2$ or CDs during the $H_2$ pretreatment process ($CO_2 + TiO_2(H)/CDs(H) \rightarrow CH + H_2O$).

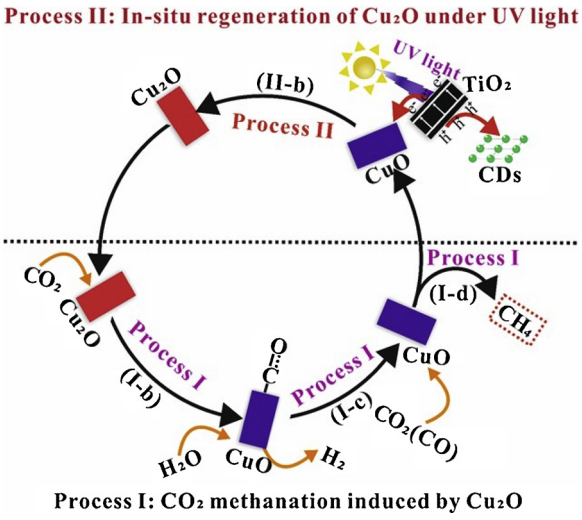


**Fig. 12.** The possible mechanism for $CO_2$ reduction by $H_2O$ over Cu/$TiO_2$-C under irradiation. There are two main processes: one is the $CO_2$ reduction by $Cu_2O$ above 150 °C (seeing the lower part), the other is the in-situ regeneration of $Cu_2O$ from CuO under UV irradiation (seeing the upper part).

As can be seen, it is the cycle of Cu(II)/Cu(I) in the structured Cu/$TiO_2$-C sample to be responsible for the excellent $CO_2$ methanation under UV irradiation. As for the reduction of CuO to $Cu_2O$ over Cu/$TiO_2$-C induced by UV light, it can be ascribed to the suitable Fermi energy level (the reduced potential) of CDs. As described in Fig. 13a, the electrons from $TiO_2$ excited by UV light can transfer to CuO, but it would further transfer to CDs due to the CDs' Fermi energy level lower than that of $Cu_2O$, resulting in $Cu_2O$ not reduced to Cu(0). Here, CDs can act as an electron reservoir to keep the stability of $Cu_2O$. However, the electrons accepted by CuO cannot further transfer to CDs due to the Fermi energy level of CuO lower that of CDs, i.e., CuO can accept the electrons from the photo-excited $TiO_2$ to form the stable $Cu_2O$. For Cu/$TiO_2$, the CuO species can be completely reduced to the Cu(0) species ($CuO + e^- \rightarrow Cu_2O + e^- \rightarrow Cu$) by the photo-excited electrons from $TiO_2$ due to no electron reservoir from CDs (seeing Fig. 13b), here, the $Cu_2O$ species are unstable over the Cu/$TiO_2$ sample.

This work shows that the non-spontaneous thermodynamic reaction ($CO_2$ reduction by $H_2O$) can be designed as two ongoing spontaneous processes ((1) $CO_2$ is reduced to CO by $Cu_2O$; (2) CO is reduced by $H_2O$) over a structured Cu/$TiO_2$-C catalyst. Moreover, the consumed $Cu_2O$ active sites can be regenerated by $TiO_2$ under UV irradiation during the reaction process. This designed reaction system by photo-thermal coupling will provide a possible new approach to achieve the efficient reduction of $CO_2$ by $H_2O$, which may be also available for other non-spontaneous or spontaneous redox reactions in thermodynamic.

## 4. Conclusions

In summary, the methanation of $CO_2$ with $H_2O$ has been realized by a designed photo-thermal configuration over the carbon dots drafted Cu/$TiO_2$ catalyst (Cu/$TiO_2$-C). The results of XPS, in-situ DRIFTS and TPSR-MS show that this non-spontaneous reaction occurs above 150 °C via three steps: (1) $CO_2$ is reduced to CO by $Cu_2O$; (2) $H_2$ is produced by a WGS reaction; (3) $CH_4$ is formed by $H_2$ reducing CO or $CO_2$, where a stable $Cu_2O$ is the key factor for the excellent activity under UV

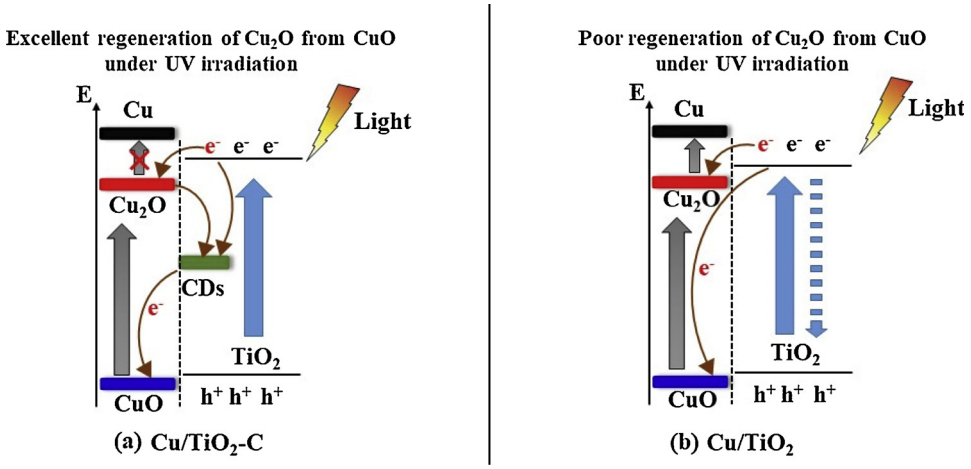


**Fig. 13.** The schematics of Cu(II) (CuO) reduction by $H_2$ or UV light over Cu/$TiO_2$-C (a) and Cu/$TiO_2$ (b). Here, the $Cu_2O$ species are stable over Cu/$TiO_2$-C due to the electron reservoir effect of CDs, but was unstable over Cu/$TiO_2$.

irradiation. Under UV irradiation, the formed CuO could be reduced to $Cu_2O$ by the photo-excited electrons from $TiO_2$ (a process of in-situ regeneration of $Cu_2O$ active sites). Here, CDs would act as an electron reservoir to store and transport the photo-excited electrons, urging an excellent cycle of CuO/$Cu_2O$ and then ensuring the continuous reaction. This work will provide some deep insights into the mechanism of $CO_2$ reduction by $H_2O$ over Cu-based catalysts in a photo-thermal reaction system, and maybe also provides a new approach to realize some non-spontaneous reactions in thermodynamic.

## Acknowledgments

This work was financially supported by the National Natural Science Foundation of China (no. 21872030) and the Science & Technology Plan Project of Fujian Province (no.2014Y2003).

## Appendix A. Supplementary data

Supplementary material related to this article can be found, in the online version, at doi:https://doi.org/10.1016/j.apcatb.2019.117780.

## References

[1] P.Y. Liou, S.C. Chen, J.C.S. Wu, D. Liu, S. Mackintosh, M. Maroto-Valerb, R. Linforth, Photocatalytic $CO_2$ reduction using an internally illuminated monolith photoreactor, Energy Environ. Sci. 4 (2011) 1487–1494.
[2] I.H. Tseng, J.C.S. Wu, H.Y. Chou, Effects of sol–gel procedures on the photocatalysis of Cu/$TiO_2$ in $CO_2$ photoreduction, J. Catal. 221 (2004) 432–440.
[3] M. Kilo, J. Weigel, A. Wokaun, R.A. Koeppel, Effect of the addition of chromium- and manganese oxides on structural and catalytic properties of copper/zirconia catalysts for the synthesis of methanol from carbon dioxide, J. Mol. Catal. A Chem. 126 (1997) 169–184.
[4] Y. Hartadi, D. Widmann, R.J. Behm, $CO_2$ hydrogenation to methanol on supported Au catalysts under moderate reaction conditions: support and particle size effects, ChemSusChem 8 (2015) 456–465.
[5] M.R. Gogate, R.J. Davis, Comparative study of CO and $CO_2$ hydrogenation over supported Rh–Fe catalysts, Catal. Commun. 11 (2001) 901–906.
[6] Q. Liu, Y. Zhou, J. Kou, X. Chen, Z. Tian, J. Guo, S. Yan, Z. Zou, High-yield synthesis of ultralong and ultrathin $Zn2GeO_4$ Nanoribbons toward improved photocatalytic reduction of $CO_2$ into renewable hydrocarbon fuel, J. Am. Chem. Soc. 132 (2010) 14385–14387.
[7] S. Xie, Y. Wang, Q. Zhang, W. Deng, Y. Wang, $SrNb_2O_6$ nanoplates as efficient photocatalysts for the preferential reduction of $CO_2$ in the presence of $H_2O$, Chem. Commun. 51 (2015) 3430–3433.
[8] Ş. Neaţu, J.A. Maciá-Agulló, P. Concepción, H. Garcia, Gold-copper nanoalloys supported on $TiO_2$ as photocatalysts for $CO_2$ reduction by water, J. Am. Chem. Soc. 136 (2014) 15969–15976.
[9] S. Kattel, B. Yan, Y. Yang, J.G. Chen, P. Liu, Optimizing binding energies of key intermediates for $CO_2$ hydrogenation to methanol over oxide-supported copper, J. Am. Chem. Soc. 138 (2016) 12440–12450.
[10] G.C. Wang, J. Nakamura, Structure sensitivity for forward and reverse water-gas shift reactions on copper surfaces: a DFT study, J. Phys. Chem. Lett. 1 (2010) 3053–3057.
[11] J. Graciani, K. Mudiyanselage, F. Xu, A.E. Baber, J. Evans, S.D. Senanayake, D.J. Stacchiola, P. Liu, J. Hrbek, J.F. Sanz, J.A. Rodriguez, Highly active copper-ceria and copper-ceria-titania catalysts for methanol synthesis from $CO_2$, SCIENCE 345 (2014) 546–550.
[12] Y. Zhou, Z. Tian, Z. Zhao, Q. Liu, J. Kou, X. Chen, J. Gao, S. Yan, Z. Zou, High-yield synthesis of ultrathin and uniform $Bi_2WO_6$ square nanoplates benefitting from photocatalytic reduction of $CO_2$ into renewable hydrocarbon fuel under visible light, ACS Appl. Mater. Interfaces 3 (2011) 3594–3601.
[13] L. Liang, X. Li, Y. Sun, Y. Tan, X. Jiao, H. Ju, Z. Qi, J. Zhu, Y. Xie, Infrared light-driven $CO_2$ overall splitting at room temperature, Joule 2 (2018) 1–13.
[14] X. Chen, Y. Zhou, Q. Liu, Z. Li, J. Liu, Z. Zou, Ultrathin, single-crystal $WO_3$ nanosheets by two-dimensional oriented attachment toward enhanced photocatalystic reduction of $CO_2$ into hydrocarbon fuels under visible light, ACS Appl. Mater. Interfaces 4 (2012) 3372–3377.
[15] S.C. Roy, O.K. Varghese, M. Paulose, C.A. Grimes, Toward solar fuels: photocatalytic conversion of carbon dioxide to hydrocarbons, ACS Nano 4 (2010) 1259–1278.
[16] K. Kocl, K. Mateju, L. Obalova, Z. Krejcikova, D. Placha, Z. Lacny, L. Capek, A. Hospodkova, O. Solcova, Effect of silver doping on the $TiO_2$ for photocatalytic reduction of $CO_2$, Appl. Catal. B 96 (2010) 239–244.
[17] S.N. Habisreutinger, L. Schmidt-Mende, J.K. Stolarczyk, Photocatalytic reduction of $CO_2$ on $TiO_2$ and other semiconductors, Angew. Chemie 52 (2013) 7372–7408.
[18] S. Xie, Y. Wang, Q. Zhang, W. Fan, W. Deng, Y. Wang, Photocatalytic reduction of $CO_2$ with $H_2O$: significant enhancement of the activity of Pt-$TiO_2$ in $CH_4$ formation by addition of MgO, Chem. Commun. 49 (2013) 2451–2453.
[19] Y. Li, W.N. Wang, Z. Zhan, M.H. Woo, C.Y. Wu, P. Biswas, Photocatalytic reduction of $CO_2$ with $H_2O$ on mesoporous silica supported Cu/$TiO_2$ catalysts, Appl. Catal. B 100 (2010) 386–392.
[20] W.N. Wang, J. Park, P. Biswas, Rapid synthesis of nanostructured Cu–$TiO_2$–$SiO_2$ composites for $CO_2$ photoreduction by evaporation driven self-assembly, Catal. Sci. Technol. 1 (2011) 593–600.
[21] R.A. Rather, S. Singh, B. Pal, A $Cu^{+1}/Cu^0$-$TiO_2$ mesoporous nanocomposite exhibits improved H2 production from $H_2O$ under direct solar irradiation, J. Catal. 346 (2017) 1–9.
[22] H. Sudrajat, P. Sujaridworakun, Insights into structural properties of Cu species loaded on $Bi_2O_3$ hierarchical structures for highly enhanced photocatalysis, J. Catal. 352 (2017) 394–400.
[23] L. Liu, C. Zhao, J.T. Miller, Y. Li, Mechanistic Study of $CO_2$ Photoreduction with $H_2O$ on Cu/$TiO_2$ nanocomposites by in Situ X-ray absorption and infrared spectroscopies, J. Phys. Chem. C 121 (2017) 490–499.
[24] S. Zhu, S. Liang, Y. Tong, X. An, J. Long, X. Fu, X. Wang, Photocatalytic reduction of $CO_2$ with $H_2O$ to $CH_4$ on Cu(I) supported $TiO_2$ nanosheets with defective {001} facets, Phys. Chem. Chem. Phys. 17 (2015) 9761–9770.
[25] R. Gusain, P. Kumar, O.P. Sharma, S.L. Jain, O.P. Khatri, Reduced graphene oxide–CuO nanocomposites for photocatalytic conversion of $CO_2$ into methanol under visible light irradiation, Appl. Catal. B 181 (2016) 352–362.
[26] P. Mirtchev, E.J. Henderson, N. Soheilnia, C.M. Yip, G.A. Ozin, Solution phase synthesis of carbon quantum dots as sensitizers for nanocrystalline $TiO_2$ solar cells, J. Mater. Chem. 22 (2012) 1265–1269.
[27] S. Zhu, J. Zhang, C. Qiao, S. Tang, Y. Li, W. Yuan, B. Li, L. Tian, F. Liu, R. Hu, H. Gao, H. Wei, H. Zhang, H. Sun, B. Yang, Strongly green-photoluminescent graphene quantum dots for bioimaging applications, Chem. Commun. 47 (2011) 6858–6860.
[28] J. Di, J. Xia, Y. Ge, H. Li, H. Ji, H. Xu, Q. Zhang, Novel visible-light-driven CQDs/$Bi_2WO_6$ hybrid materials with enhanced photocatalytic activity toward organic pollutants degradation and mechanism insight, Appl. Catal. B 168–169 (2015) 51–61.
[29] H. Zhang, H. Ming, S. Lian, H. Huang, H. Li, L. Zhang, Y. Liu, Z. Kang, S.T. Lee,

$Fe_2O_3$/carbon quantum dots complex photocatalysts and their enhanced photocatalytic activity under visible light, J. Chem. Soc. Dalton Trans. 40 (2011) 10822–10825.
[30] B.Y. Yu, S.Y. Kwak, Carbon quantum dots embedded with mesoporous hematite nanospheres as efficient visible light-active photocatalysts, J. Mater. Chem. 22 (2012) 8345–8353.
[31] M. Tahir, B. Tahir, N.A.S. Amin, H. Alias, Selective photocatalytic reduction of $CO_2$ by $H_2O/H_2$ to $CH_4$ and $CH_3OH$ over Cu-promoted $In_2O_3/TiO_2$ nanocatalyst, Appl. Surf. Sci. 389 (2016) 46–55.
[32] K. Ikeue, S. Nozaki, M. Ogawa, M. Anpo, Photocatalytic reduction of $CO_2$ with $H_2O$ on Ti-containing porous silica thin film photocatalysts, Catal. Letters 80 (2002) 111–114.
[33] Q.H. Zhang, W.D. Han, Y.J. Hong, J.G. Yu, Photocatalytic reduction of $CO_2$ with $H_2O$ on Pt-loaded $TiO_2$ catalyst, Catal. Today 148 (2009) 335–340.
[34] Y. Wang, B. Li, C. Zhang, L. Cui, S. Kang, X. Li, L. Zhou, Ordered mesoporous $CeO_2$-$TiO_2$ composites: highly efficient photocatalysts for the reduction of $CO_2$ with $H_2O$ under simulated solar irradiation, Appl. Catal. B 130–131 (2013) 277–284.
[35] S. Zhu, Q. Meng, L. Wang, J. Zhang, Y. Song, H. Jin, K. Zhang, H. Sun, H. Wang, B. Yang, Highly photoluminescent carbon dots for multicolor patterning, sensors, and bioimaging, Angew. Chemie 52 (2013) 3953–3957.
[36] Y. Huang, Y. Liang, Y. Rao, D. Zhu, J.J. Cao, Z. Shen, W. Ho, S.C. Lee, Environment-friendly carbon quantum Dots/$ZnFe_2O_4$ photocatalysts: characterization, biocompatibility, and mechanisms for NO removal, Environ. Sci. Technol. 51 (2017) 2924–2933.
[37] Slamet, H.W. Nasution, E. Purnama, S. Kosela, J. Gunlazuardi, Photocatalytic reduction of $CO_2$ on copper-doped titania catalysts prepared by improved-impregnation method, Catal. Commun. 6 (2005) 313–319.
[38] K. Yang, J. Liu, R. Si, X. Chen, W. Dai, X. Fu, Comparative study of Au/$TiO_2$ and Au/$Al_2O_3$ for oxidizing CO in the presence of $H_2$ under visible light irradiation, J. Catal. 317 (2014) 229–239.
[39] P.N. Paulino, V.M.M. Salim, N.S. Resende, Zn-Cu promoted $TiO_2$ photocatalyst for $CO_2$ reduction with $H_2O$ under UV light, Appl. Catal. B 185 (2016) 362–370.
[40] Z. Wang, D. Brouri, S. Casale, L. Delannoy, C. Louis, Exploration of the preparation of Cu/$TiO_2$ catalysts by deposition–precipitation with urea for selective hydrogenation of unsaturated hydrocarbons, J. Catal. 340 (2016) 95–106.
[41] L. Liu, H. Zhao, J.M. Andino, Y. Li, Photocatalytic $CO_2$ Reduction with $H_2O$ on $TiO_2$ nanocrystals: comparison of anatase, rutile, and brookite polymorphs and exploration of surface chemistry, ACS Catal. 2 (2012) 1817–1828.
[42] L. Lin, K. Wang, K. Yang, X. Chen, X. Fu, W. Dai, The visible-light-assisted thermocatalytic methanation of $CO_2$ over Ru/$TiO_{(2-x)}N_x$, Appl. Catal. B 204 (2017) 440–455.
[43] M. Park, B.S. Kwak, S.W. Jo, M. Kang, Effective $CH_4$ production from $CO_2$ photoreduction using $TiO_2$/xmol% Cu–$TiO_2$ double-layered films, Energy Convers. Manage. 103 (2015) 431–438.
[44] J. Zhao, Y. Li, Y. Zhu, Y. Wang, C. Wang, Enhanced $CO_2$ photoreduction activity of black $TiO_2$-coated Cu nanoparticles under visible light irradiation: role of metallic Cu, Appl. Catal. A Gen. 510 (2016) 34–41.
[45] X.Y. Kong, W.L. Tan, B.J. Ng, S.P. Chai, A.R. Mohamed, Harnessing Vis–NIR broad spectrum for photocatalytic $CO_2$ reduction over carbon quantum dots-decorated ultrathin $Bi_2WO_6$ nanosheets, Nano Res. 10 (2017) 1720–1731.
[46] G. Silversmit, H. Poelman, D. Depla, N. Barrett, G.B. Marin, R.D. Gryse, A comparative XPS and UPS study of $VO_x$ layers on mineral $TiO_2$(001)-anatase supports, Surf. Interface Anal. 38 (2003) 1257–1265.
[47] P. Liu, E.J. Hensen, Highly efficient and robust Au/$MgCuCr_2O_4$ catalyst for gas-phase oxidation of ethanol to acetaldehyde, J. Am. Chem. Soc. 135 (2013) 14032–14035.
[48] M.C. Biesinger, L.W.M. Lau, A.R. Gerson, R.S.C. Smart, Resolving surface chemical states in XPS analysis of first row transition metals, oxides and hydroxides: Sc, Ti, V, Cu and Zn, Appl. Surf. Sci. 257 (2010) 887–898.
[49] N.L. Reddy, S. Kumarb, V. Krishnan, M. Sathish, M.V. Shankar, Multifunctional Cu/Ag quantum dots on $TiO_2$ nanotubes as highly efficient photocatalysts for enhanced solar hydrogen evolution, J. Catal. 350 (2017) 226–239.
[50] F. Boccuzzi, A. Chiorino, M. Manzoli, D. Andreeva, T. Tabakova, FTIR study of the low-temperature water–gas shift reaction on Au/$Fe_2O_3$ and Au/$TiO_2$ Catalysts, J. Catal. 188 (1999) 176–185.
[51] I. Tankov, W.H. Cassinelli, J.M.C. Bueno, K. Arishtirova, S, Damyanova, DRIFTS study of CO adsorption on praseodymium modified Pt/$Al_2O_3$, Appl. Surf. Sci. 259 (2012) 831–839.
[52] K. Teramura, T. Tanaka, H. Ishikawa, Y. Kohno, T. Funabiki, Photocatalytic reduction of $CO_2$ to CO in the presence of $H_2$ or $CH_4$ as a reductant over MgO, J. Phys. Chem. B 108 (2004) 346–354.
[53] I. Nakamura, H. Nakano, T. Fujitani, T. Uchijima, J. Nakamura, Evidence for a special formate species adsorbed on the Cu–Zn active site for methanol synthesis, Surf. Sci. 402–404 (1998) 92–95.
[54] C.P.L. Regli, J.G. Vitillo, F. Bonino, A. Damin, C. Lamberti, A. Zecchina, P.L. Solari, K.O. Kongshaug, S. Bordiga, Local structure of framework Cu(II) in HKUST-1 metallorganic framework: spectroscopic characterization upon activation and Interaction with adsorbates, Chem. Mater. 18 (2006) 1337–1346.
[55] F. Giordanino, P.N.R. Vennestrom, L.F. Lundegaard, F.N. Stappen, S. Mossin, P. Beato, S. Bordiga, C. Lamberti, Characterization of Cu-exchanged SSZ-13: a comparative FTIR, UV-Vis, and EPR study with Cu-ZSM-5 and Cu-beta with similar Si/Al and Cu/Al ratios, J. Chem. Soc. Dalton Trans. 42 (2013) 12741–12761.
[56] M. Zhu, T.C.R. Rocha, T. Lunkenbein, A. Knop-Gericke, R. Schlogl, I.E. Wachs, Promotion mechanisms of iron oxide-based high temperature water-gas shift catalysts by chromium and copper, ACS Catal. 6 (2016) 4455–4464.
[57] J.B. Parise, B. Theroux, R. Li, J.S. Loveday, W.G. Marshall, S. Klotz, Pressure dependence of hydrogen bonding in metal deuteroxides: a neutron powder diffraction study of $Mn(OD)_2$ and β-$Co(OD)_2$, Phys. Chem. Minerals 25 (1998) 130–137.
[58] R.W.R.V. Stevens Siriwardane Jr., J. Logan, In situ fourier transform infrared (FTIR) investigation of $CO_2$ adsorption onto zeolite materials, s, Energy Fuel 22 (2008) 3070–3079.
[59] W. Huang, K.C. Xie, J.P. Wang, Z.H. Gao, L.H. Yin, Q.M. Zhu, Possibility of direct conversion of $CH_4$ and $CO_2$ to high-value products, J. Catal. 201 (2011) 100–104.
[60] A. Bansode, B. Tidona, P.R. von Rohrb, A. Urakawa, Impact of K and Ba promoters on $CO_2$ hydrogenation over Cu/$Al_2O_3$ catalysts at high pressure, Catal. Sci. Technol. 3 (2013) 767–778.
[61] X. Wang, L. Andrews, L. Manceron, C. Marsden, Infrared spectra and DFT calculations for the coinage metal hydrides MH, $(H_2)$ MH, $MH_2$, $M_2H$, $M_2H$-, and $(H_2)$CuHCu in solid argon, neon, and hydrogen, J. Phys. Chem. A 107 (2003) 8492–8505.
[62] K.K. Bando, K. Sayama, H. Kusama, K. Okabe, H. Arakawa, In-situ FT-IR study on $CO_2$ hydrogenation over Cu catalysts supported on $SiO_2$, $Al2O_3$, and $TiO_2$, Appl. Catal. A Gen. 165 (1997) 391–409.